

# Tuning the orbital-lattice fluctuations in the mixed spin-dimer system $\text{Ba}_{3-x}\text{Sr}_x\text{Cr}_2\text{O}_8$

Alsu Gazizulina,<sup>1,\*</sup> Diana Lucia Quintero-Castro,<sup>2,3</sup> Dirk Wulferding,<sup>4,5</sup>  
Jeremie Teyssier,<sup>6</sup> Karel Prokes,<sup>3</sup> Fabiano Yokaichiya,<sup>3</sup> and Andreas Schilling<sup>1</sup>

<sup>1</sup>Physik-Institut, Universität Zürich, 8057 Zürich, Switzerland

<sup>2</sup>Department of Mathematics and Physics, University of Stavanger, 4036 Stavanger, Norway

<sup>3</sup>Helmholtz Zentrum Berlin für Materialien und Energie, 14109 Berlin, Germany

<sup>4</sup>Institute for Condensed Matter Physics, TU Braunschweig, 38106 Braunschweig, Germany

<sup>5</sup>Laboratory for Emerging Nanometrology (LENA), TU Braunschweig, 38106 Braunschweig, Germany

<sup>6</sup>Department of Quantum Matter Physics, University of Geneva, 1211 Geneva, Switzerland

In  $\text{A}_3\text{Cr}_2\text{O}_8$ , where  $\text{A} = \text{Sr}$  or  $\text{Ba}$ , the  $\text{Cr}^{5+}$  ions surrounded by oxygen ions in a tetrahedral coordination are Jahn-Teller active. The Jahn-Teller distortion leads to a structural transition and a related emergence of three twinned monoclinic domains below the structural phase transition. This transition is highly *dynamic* over an extended temperature range for  $\text{A} = \text{Sr}$ . We have investigated mixed compounds  $\text{Ba}_{3-x}\text{Sr}_x\text{Cr}_2\text{O}_8$  with  $x = 2.9$  and  $x = 2.8$  by means of X-ray and neutron diffraction, Raman scattering and calorimetry. Based on the obtained evolution of the phonon frequencies, we find a distinct suppression of the orbital-lattice fluctuation regime with increasing Ba content. This stands in contrast to the linear behaviour exhibited by unit cell volumes, atomic positions and intradimer spin-spin exchange interactions.

## INTRODUCTION

In many condensed matter systems, e.g. manganites, ferrites, cuprates, among others, the key to functional magneto-electronic properties is the interaction between degenerate orbital degrees of freedom and lattice fluctuations through a cooperative Jahn-Teller effect [1–6]. This effect can eventually change the crystallographic structure, fully lift the orbital degeneracy or create a short-range orbital order through a dynamical Jahn-Teller distortion. Spin-spin correlations are also relevant in these strongly correlated compounds, and can interact with orbital and lattice degrees of freedom. Even more, interesting dynamics can emerge when the spin-spin correlations are spatially frustrated, leading to a macroscopic degeneracy of the ground state [7].

All these competing degrees of freedom are present in  $\text{A}_3\text{Cr}_2\text{O}_8$  (with  $\text{A} = \text{Ba}$ ,  $\text{Sr}$ ). These systems consist of a 3-dimensional network of coupled spin dimers formed by the Jahn-Teller active ion,  $\text{Cr}^{5+}$ . The dimers form hexagonal bilayers and are antiferromagnetically linked in a triangular in-plane arrangement, resulting in a certain degree of magnetic frustration. In an earlier work, Raman scattering experiments were performed on a single crystal of  $\text{Sr}_3\text{Cr}_2\text{O}_8$  [8]. An extended orbital-lattice fluctuation regime was detected and related to structural distortion, orbital ordering and further changes in the orbital sector below the Jahn-Teller transition temperature  $T_{JT}$ . At this temperature,  $T_{JT} = 285$  K for  $\text{Sr}_3\text{Cr}_2\text{O}_8$  and  $T_{JT} = 70$  K for  $\text{Ba}_3\text{Cr}_2\text{O}_8$ , the structural transition from hexagonal  $R\bar{3}m$  to monoclinic  $C2/c$  symmetry appears in both compounds (Fig. 1) [9]. There is no fluctuation regime in the lattice degrees of freedom in  $\text{Ba}_3\text{Cr}_2\text{O}_8$  [10] as the orbital entropy associated with the splitting of the orbital ground state is completely recovered at the Jahn-Teller transition. These differences in the dynamic orbital properties between these two systems stand in contrast to the magnetic ground state (singlet) and magnetic excitations (triplons) which are essentially similar in both compounds [11, 12].

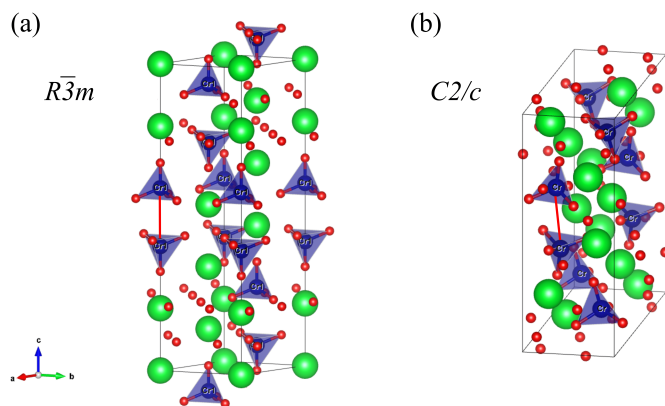


FIG. 1: (Color online) (a) Hexagonal and (b) monoclinic unit cells in  $\text{A}_3\text{Cr}_2\text{O}_8$ .  $\text{Cr}^{5+}$  ions, represented in blue, are located in oxygen tetrahedra,  $\text{O}^{2-}$  ions are represented by red spheres and  $\text{A} = \text{Sr/Ba}$  by green spheres. Dimer bonds are represented in red

It is known that by mixing different cations in the atomic structure of functional materials, weak disorder can be introduced and it may be sufficient to change physical properties dramatically [4, 13]. Many exotic phases can be observed in mixed condensed matter electronic systems, such as perovskites [14] and cuprates [5], where unusual strong orbital-lattice coupling has been observed [15]. The abundance of functional properties in those mixed systems is stimulated by a static displacive disorder due to differences in ionic radii, which creates mixed charge distribution [16]. However, the complex magnetic phase diagrams by settling of very different long range magnetic order as a function of cation mixing present in many of these compounds, make the direct study of the orbital dynamics non-trivial.

Recently, we reported on the effect of chemical substitution on the magnetic properties of  $\text{Ba}_{3-x}\text{Sr}_x\text{Cr}_2\text{O}_8$  upon partially replacing Sr by Ba by 3.3% and 6.6%. It was found that the

intradimer spin-spin interaction is smaller in the mixed compound with  $x = 2.9$  than in pure  $\text{Sr}_3\text{Cr}_2\text{O}_8$  by 4%, whereas the interdimer exchange interactions are reduced by 7% [17]. No sign of magnetic disorder was found. Furthermore, we have found that the critical magnetic field related to the condensation of the triplet magnetic excitations decreases monotonically with  $x$  [18]. This change is in accordance with the change the intra-dimer interaction constant  $J_0$  [19].

Here, we report the study of the *dynamic* structural phase distortions in the mixed systems  $\text{Ba}_{3-x}\text{Sr}_x\text{Cr}_2\text{O}_8$  (with  $x = 2.8, 2.9$ ). Both pristine and mixed compounds preserve the magnetic ground state and are therefore the ideal model systems to study uniquely orbit-lattice fluctuations as a function of cation mixing. We investigated the structural phase transition in the mixed compounds over an extended temperature range. Using heat capacity measurements, Raman scattering, neutron single crystal diffraction and high-resolution X-ray powder diffraction techniques, we have explored the variation of the crystal structure of  $\text{Ba}_{3-x}\text{Sr}_x\text{Cr}_2\text{O}_8$  (with  $x = 2.9$  and  $x = 2.8$ ) as a function of temperature.

## EXPERIMENTAL DETAILS

Single crystals of  $\text{Ba}_{3-x}\text{Sr}_x\text{Cr}_2\text{O}_8$  were grown with  $x = 2.9$  and  $x = 2.8$ , as described in Ref. [17]. Heat capacity measurements were performed in a Physical Property Measurement System (PPMS, Quantum Design Inc.).

The temperature dependent high-resolution powder X-ray diffraction experiments were carried out at the Swiss-Norwegian beamline BM01 at the ESRF in Grenoble [20]. Temperature control was achieved using a liquid nitrogen cryostream. A powder sample of  $\text{Ba}_{0.1}\text{Sr}_{2.9}\text{Cr}_2\text{O}_8$  was measured in the temperature range from 100 K to 300 K. To extract crystallographic lattice parameters and atomic displacement positions, Rietveld refinement was performed using the FullProf software [21].

The nuclear structure of the spin dimer system  $\text{Ba}_{3-x}\text{Sr}_x\text{Cr}_2\text{O}_8$  with  $x = 2.9$  was studied by performing single crystal neutron diffraction on the 2-axis-diffractometer E4 at the Helmholtz Zentrum für Materialien und Energie in Berlin. The sample with volume  $\cong 1 \text{ cm}^3$  was mounted with  $(h, h, l)_h$  in the scattering plane (subindices  $h$  and  $m$  correspond to hexagonal and monoclinic notation, respectively). The incident wavelength was 2.4 Å. Measurements of intensities of key Bragg peaks were made at temperatures between 1.5 K and 290 K.

Raman scattering experiments were performed using an excitation wavelength of  $\lambda = 514.5 \text{ nm}$  on single crystals of  $\text{Ba}_{3-x}\text{Sr}_x\text{Cr}_2\text{O}_8$  with  $x = 2.9$  and  $x = 2.8$ . Samples were embedded in a silver matrix to achieve better thermalization. Both crystals were mounted and polished parallel to the  $ac$  plane. The incoming laser polarization was along the  $c$  axis and scattered light of all polarizations was detected. The laser power was set to 0.5 mW with a spot diameter of about 2  $\mu\text{m}$ . Scans were recorded in 10 K steps from 5 K up to 200 K,

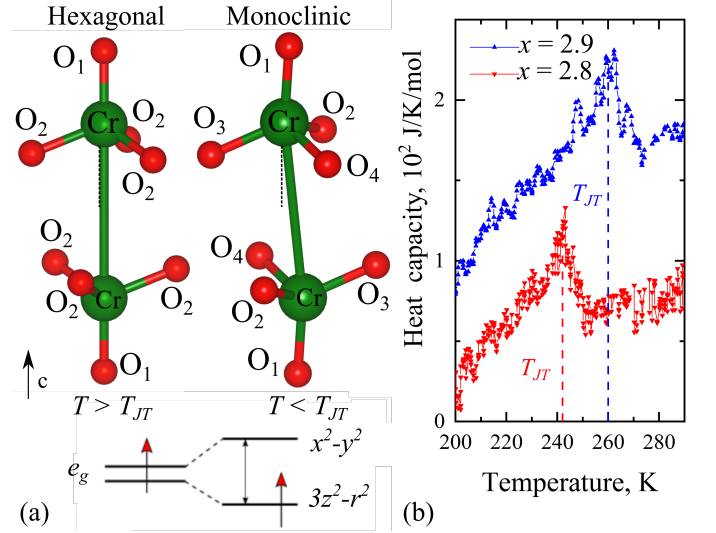


FIG. 2: (Color online) (a) Two  $\text{CrO}_4$  tetrahedra forming a dimer unit in the hexagonal and the monoclinic phases (top). Corresponding occupation of electronic levels in each phase (bottom). (b) Heat capacity-temperature dependences for both samples:  $x = 2.9$  (black curve) and  $x = 2.8$  (red curve) showing  $\lambda$ -like JT-transitions at 260 K and 242 K, respectively.

followed by 20 K steps in the range 200 K to 340 K.

## RESULTS AND DISCUSSION

In the mixed compounds  $\text{Ba}_{3-x}\text{Sr}_x\text{Cr}_2\text{O}_8$ , the magnetic ion  $\text{Cr}^{5+}$  is surrounded by four oxygen ions in a tetrahedral symmetry, as shown in Fig. 2(a). A cooperative Jahn-Teller distortion lifts the electronic degeneracy of tetrahedrally coordinated  $\text{Cr}^{5+}$  ions. At  $T > T_{JT}$ , the structure is hexagonal in the space group  $R\bar{3}m$ . Bilayers of  $\text{CrO}_4$  tetrahedra form a frustrated arrangement of two degenerate  $3d^1$   $e_g$  levels ( $3z^2 - r^2$  and  $x^2 - y^2$ ). Each orbital is coupled to the displacement of the O atoms surrounding the ion. For  $T < T_{JT}$ , crystallographic distortions lead to the monoclinic structure  $C2/c$  and a splitting of the levels of the lower-lying orbitals. This structural transition is characterised by an antiferro-distortive displacement of the apical O<sub>1</sub> oxygen ions and a slight rotation of the O<sub>2</sub> ions in the tetrahedral bottom plane within each dimer. It leads to three twinned monoclinic domains in the parent compounds  $\text{Sr}_3\text{Cr}_2\text{O}_8$  [11] and  $\text{Ba}_3\text{Cr}_2\text{O}_8$  [12].

Recently, we showed that introducing Ba in the  $\text{Sr}_3\text{Cr}_2\text{O}_8$  system does neither lead to magnetic disorder nor to intra-gap intensities in the dispersion relation [17]. The Jahn-Teller distortion temperature in  $\text{Ba}_{3-x}\text{Sr}_x\text{Cr}_2\text{O}_8$  is gradually suppressed with decreasing  $x$ , as shown in Ref. [22], and vanishes for intermediate stoichiometries  $x$ . This transition is reflected as a  $\lambda$ -like transition in the heat capacity, as measured for  $x = 2.9$  and  $x = 2.8$  [Fig. 2(b)]. For the mixed compounds

$x = 2.9$  and  $x = 2.8$ , the Jahn-Teller transition temperatures are  $T_{JT} = 260$  K and 242 K, whereas for the pure  $\text{Sr}_3\text{Cr}_2\text{O}_8$   $T_{JT}$  is 285 K and 70 K for  $\text{Ba}_3\text{Cr}_2\text{O}_8$ , respectively [8, 12].

In the X-ray powder diffraction patterns, obtained at temperatures above  $T_{JT}$  for  $x = 2.9$  compound, the observed Bragg reflections were indexed using the space group  $R\bar{3}m$ . Our analysis of those patterns shows that the lattice at  $T < T_{JT}$  is then better described using the space group  $C2/c$ , however, with new diffraction peaks gradually appearing as can be seen in Fig. 3(a). Our results are in agreement with density functional theory calculations of the orbital ordering in  $\text{Sr}_3\text{Cr}_2\text{O}_8$  that demonstrate the strong electron correlation which arises within the  $3d^1$  shell and can clearly explain a phase transition leading to the stabilisation of its monoclinic  $C2/c$  space-group symmetry and spin-singlet magnetic ground state [23].

The crystallographic parameters extracted by using Rietveld refinement [21] are presented in Table I. The weighted profile  $R$ -factor shows a relatively good fit. The lattice parameters and unit cell volume shrink in a non-linear manner as a function of temperature (Figure 3(b)). Apart from the unit cell volume and lattice constants, the structural distortion also affects the monoclinic angle  $\beta$ . The monoclinic angle decreases non-linearly by  $\Delta\beta \approx 0.12^\circ$  when increasing the temperature from 80 K to 220 K, as can be seen in Fig. 3(b), and deviates slightly from the value that is expected from a conversion between the rhombohedral and the monoclinic space groups [19].

The structural distortion is characterized by an antiferro-distortive displacement of the apical  $\text{O}_1$  oxygen ion within the  $\text{CrO}_4$  tetrahedra similar to  $\text{Sr}_3\text{Cr}_2\text{O}_8$  [9]. The displacement of  $\text{O}_1$  is coupled to the displacement of the  $\text{Sr}_1/\text{Ba}_1$  and a slight rotation of the tetrahedral basal plane, spanned by the  $\text{O}_2$  ions. This rotation and distortion further modifies the Cr-O distances below  $T_{JT}$  to  $\text{O}_2$ ,  $\text{O}_3$  and  $\text{O}_4$ . A modification of the Cr-O distances leads to a change in energy of the electronic orbitals of  $\text{Cr}^{5+}$ . The crystalline electric field splits the 3d orbitals of the  $\text{Cr}^{5+}$  ion into lower-lying non-bonding  $e_g$  orbitals and higher-lying anti-bonding  $t_{2g}$  orbitals. This distortion reduces the point group symmetry of the  $\text{Cr}^{5+}$  site from  $C_{3v}$  (in Schoenflies notation) in the hexagonal structure to  $C_1$  in the monoclinic structure where the  $e_g$  state degeneracy is lifted, with a separation into  $(3z^2 - r^2)$  and  $(x^2 - y^2)$  orbitals. The oxygen tetrahedron around the  $\text{Cr}^{5+}$  ion is only slightly affected by varying the temperature and changes only with the onset of the structural transition at  $T_{JT}$ .

Single crystal neutron diffraction was also performed in order to obtain detailed information about the formation of three monoclinic twins by measuring key reflections in the  $(h, h, l)_h$  plane, which correspond to a unique, double or triple twin, as a function of temperature. The results are shown as an inset in Figure 3(a). Three reflections were measured:  $(1, 1, -3)_h$ ,  $(1, 1, -1.5)_h$  and  $(0, 0, 6)_h$ . The reflection  $(1, 1, -1.5)_h$  corresponds to two different monoclinic reflections  $(1, 1, -1.5)_h = (0, 2, 1)_{m(1,2)} = (3, 1, 2)_{m(3)}$ , where the  $m^{(n)}$  notation corresponds to  $n^{\text{th}}$  monoclinic twin. The reflection  $(0, 0, 6)_h$  corresponds to three monoclinic twins  $(0, 0, 6)_h = (0, 0, 4)_{m(1,2,3)}$  and it is an

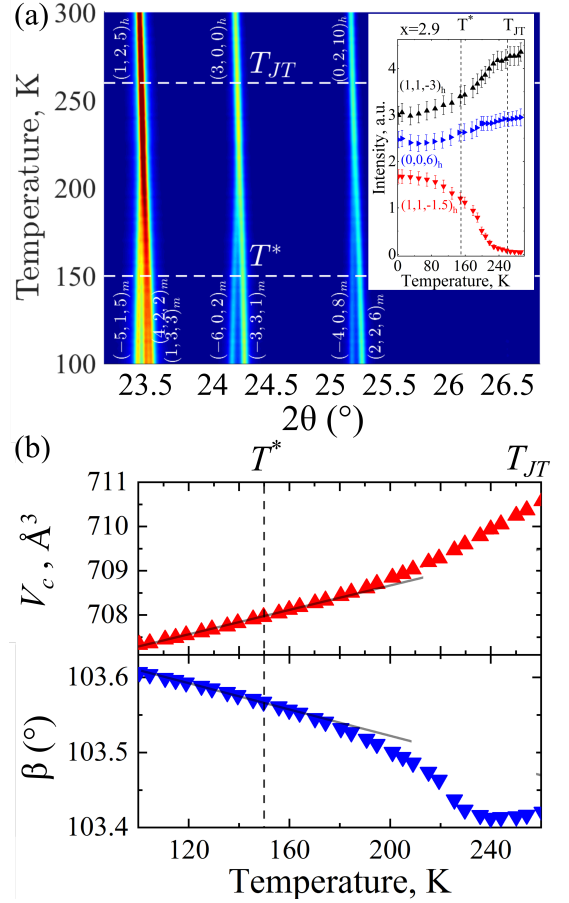


FIG. 3: (Color online) (a) Colour contour plot of the temperature dependence of the X-ray diffraction pattern for  $x = 2.9$  powder. The centred reflection  $(3, 0, 0)_h$  splits into  $(-6, 0, 2)_m$  and  $(-3, 3, 1)_m$  at lower temperatures. Inset: Temperature dependence of the integrated intensity of  $(1, 1, -3)_h$ ,  $(1, 1, -1.5)_h$  and  $(0, 0, 6)_h$  reflections of a  $x = 2.9$  single crystal. Dotted lines show  $T_{JT} = 260$  K and  $T^* = 150$  K. (b) The unit cell volume and monoclinic angle  $\beta$  in the monoclinic symmetry  $C2/c$  as a function of temperature (red and blue data points, respectively). The lines are guides to the eye

allowed hexagonal reflection, and the  $(1, 1, -3)_h$  reflection is allowed in both hexagonal and monoclinic and corresponds to the reflections  $(1, 1, -3)_h = (0, 2, 2)_{m(1)} = (3, 1, 3)_{m(2,3)}$ . Conversions from hexagonal to monoclinic Miller indices have been done following following Ref. [11]. The largest changes of the diffraction patterns are observed for temperatures far below the Jahn-Teller transition temperature  $T_{JT}$  reaching full intensities well below  $T_{JT}$ . The observed dependences indicate that the structure stabilizes below some characteristic temperature  $T^* < T_{JT}$ , which we define more precisely further below.

Fig. 4(a) shows two Raman spectra collected at 310 K and 10 K. At low temperatures two modes develop between 310 and 340  $\text{cm}^{-1}$ . They are rather broad as compared to other peaks. This indicates a possible mixing of the orbital exci-

TABLE I: Crystallographic parameters extracted from the Rietveld refinement of the BM01 data for  $x = 2.9$ . The weighted profile  $R$ -factor is  $R_{wp} \cong 8$  for both refinements, at  $T < T_{JT}$  and at  $T > T_{JT}$ .

$x = 2.9$	$C2/c$ (100 K)		$R\bar{3}m$ (300 K)	
$a$ [Å]	9.60(8)		5.57(7)	
$b$ [Å]	5.51(6)		5.57(7)	
$c$ [Å]	13.72(7)		20.20(6)	
$\alpha$ [deg]	90		90	
$\beta$ [deg]	$\cong 103.61(3)$		90	
$\gamma$ [deg]	90		120	
Atom	Atomic position $[x, y, z]_m$	$B_{iso\ m}$	Atomic position $[x, y, z]_h$	$B_{iso\ h}$
Cr	[0.2028, 0.2557, 0.8576]	0.84(7)	[0, 0, 0.4052]	0.79(9)
Sr <sub>1</sub> /Ba <sub>1</sub>	[0, 0.2715, 0.2500]	0.46(1)	[0, 0, 0]	0.79(9)
Sr <sub>2</sub> /Ba <sub>2</sub>	[0.1020, 0.2482, 0.5550]	0.42(8)	[0, 0, 0.2037]	0.64(9)
O <sub>1</sub>	[0.1602, 0.3086, 0.7386]	0.38(5)	[0, 0, 0.3255]	0.97(8)
O <sub>2</sub>	[0.8624, -0.0091, 0.6078]	0.42(4)	[0.8353, 0.1647, 0.8981]	0.97(8)
O <sub>3</sub>	[0.1143, 0.7842, 0.5987]	0.85(6)		
O <sub>4</sub>	[0.3683, 0.9842, 0.5833]	0.61(2)		

tation and a phonon. A factor group analysis [8] gives the number of Raman active phonons that was analysed for the parent compound  $\text{Sr}_3\text{Cr}_2\text{O}_8$ . 11 Raman active phonon modes are expected in the hexagonal symmetry  $R\bar{3}m$  and 39 corresponding modes in the monoclinic space group  $C2/c$ . The respective mode frequencies and their symmetry assignments are given in Ref. [8]. We detected only slight shifts in the phonon frequencies when compared with the parent compound  $\text{Sr}_3\text{Cr}_2\text{O}_8$ .

We observe distinct changes in the phonon spectra in the temperature range 100 K - 260 K [see Figs. 4(b) and 4(c)]. Below a temperature around 150 K ( $T^*$ ) for  $x = 2.9$ , the quasi-elastic scattering (seen as a subtle increase in scattering intensity towards low energies) is suppressed and the Raman spectra show a behaviour that can be described as a stabilisation of the lattice. Therefore,  $T^*$  marks a crossover from orbital fluctuations to long-range and static structural distortions and we can therefore interpret the temperature window between  $T^*$  and  $T_{JT}$  as a range with strong fluctuations. The strong electron correlation arising within the  $3d$  shell of  $\text{Cr}^{5+}$  can explain the phase transition leading to the stabilisation of the monoclinic  $C2/c$  space group symmetry.

Taking a closer look at the phonon mode around  $140\text{ cm}^{-1}$ , the transition is very smooth between 200 K and 150 K in the case of  $x = 2.9$ , whereas for  $x = 2.8$  there seems to be a sudden jump around 125 K [see marks in Figs. 4(b) and 4(c)]. We can conclude that there is a slightly different fluctuating behaviour for the lattice of two compounds. In Fig. 4(d, e), the frequencies of the phonon modes, extracted with a Lorentz fitting, are plotted as a function of temperature. Both samples,  $x = 2.9$  and  $x = 2.8$ , show similar trends in their temperature evolution with a strong softening of the  $3A_g$  modes at about 70, 90 and  $105\text{ cm}^{-1}$ . In particular, the mode around  $70\text{ cm}^{-1}$  evidences a dramatic softening upon increasing the temperature towards  $T^*$  due to a strong coupling to electronic degrees of freedom. This mode is very susceptible to the atomic displacement of the apical oxygen  $\text{O}_1$  in the  $\text{CrO}_4$ -

tetrahedra, and the related displacement may correspond to a possible rotational motion of the  $\text{CrO}_4$ -tetrahedra that modifies all Cr-O distances. Therefore, once the Jahn-Teller distortion changes the transition from dynamic to static at  $T^*$ , this soft mode starts to emerge. This process can be viewed as a static tetrahedral distortion. Thus, we can consider this phonon energy as a secondary order parameter, that emerges from orbital order and can be described by mean-field theory,  $\omega(T) = A |T^* - T|^\eta$  (see fits in Fig. 4(d, e)), where  $\eta$  denotes the critical exponent of the secondary order parameter and  $T^*$  indicates the critical temperature of the transition [25]. We obtain  $\eta = 0.12$  and  $0.16$  for  $x = 2.9$  and  $x = 2.8$ , respectively. These exponents are close to the two-dimensional Ising solution where  $\eta = 1/8$ . A similar mean-field exponent has been extracted from a soft phonon mode in the related Jahn-Teller active  $\text{BaNa}_2\text{Fe}[\text{VO}_4]_2$  [24].

Based on the mean-field fit to the soft mode energy  $70\text{ cm}^{-1}$ , we obtain  $T^* = (150 \pm 3)\text{ K}$  for  $x = 2.9$  and  $T^* = (170 \pm 5)\text{ K}$  for  $x = 2.8$ . Interestingly,  $T^*$  for  $x = 2.8$  is noticeably enhanced in comparison with  $x = 2.9$ . This means that the fluctuation regime is narrowed with increasing Ba content and fluctuations are suppressed. Fig. 5 shows the temperature range of the fluctuation regime  $|T_{JT} - T^*|$  and the intra-dimer magnetic exchange interaction  $J_0$  as a function of Sr content  $x$  in  $\text{Ba}_{3-x}\text{Sr}_x\text{Cr}_2\text{O}_8$ . Values for the end members  $\text{Ba}_3\text{Cr}_2\text{O}_8$  and  $\text{Sr}_3\text{Cr}_2\text{O}_8$  are taken from literature [8, 10]. The interaction  $J_0$  changes monotonously in the shown region of  $x$  but not linearly as the lattice parameters [19]. The area below the data points of the temperature range  $|T_{JT} - T^*|$  marked by yellow color is a guide for the eye. It shows that the fluctuation regime decreases drastically and would vanish around  $x = 2.72$ .

There are different plausible scenarios leading to a decrease in  $T_{JT}$  and a suppression of the fluctuation regime upon increasing Ba content: One possibility could be some disorder or bond length mixing induced by Ba/Sr substitution. However, our experiments evidence a systematic trend, where the



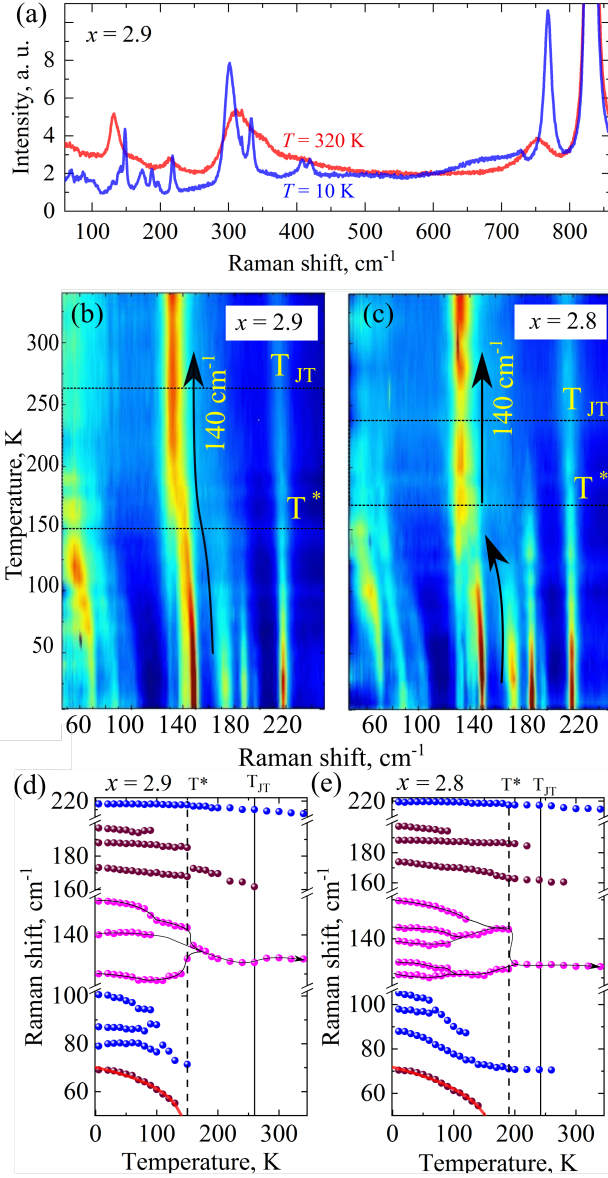


FIG. 4: (Color online) (a) Raman spectra collected at  $T = 320$  K (red curve) and at 10 K (blue curve) for  $x = 2.9$ . Colour plot spectra in the temperature range from 5 K to 340 K for (b)  $x = 2.9$  and (c)  $x = 2.8$ . Temperature evolution of the phonon frequencies for (d)  $x = 2.9$  and (e)  $x = 2.8$ . The red line is a fit of the mode around  $70 \text{ cm}^{-1}$ .

end members (with the lowest level of disorder) mark the two extreme cases of no fluctuations vs. maximum fluctuations. Since lattice constants and unit cell volume change linearly [19] as a function of  $x$ , there is also no obvious structural reason for the suppression of  $T^*$ . A more likely scenario is a continuous tuning of the intradimer interaction  $J_0$  (shown on the right axis of Fig. 5) as well as the ratio of inter- to intradimer interaction  $J'/J_0$  with  $x$ . In fact it was found that for  $\text{Ba}_3\text{Cr}_2\text{O}_8$  this ratio is slightly larger ( $J'/J_0 = 0.82$ ) than for  $\text{Sr}_3\text{Cr}_2\text{O}_8$  ( $J'/J_0 = 0.64$ ) [17]. This subtle difference could

be the reason for the fundamentally different dynamics. An observed stronger interdimer coupling  $J'$  (with respect to  $J_0$ ) can lead to a faster stabilization of the spin- and the orbital subsystem, whereas a weaker interdimer coupling preserves a low-dimensional quantum magnetism character of the spin dimer system, which is more prone to strong fluctuations.

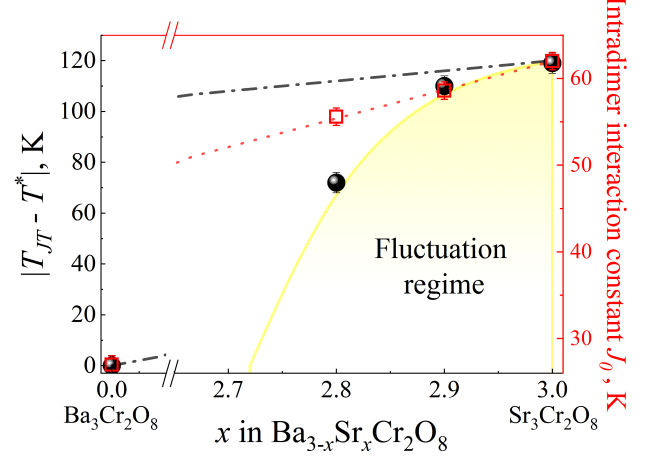


FIG. 5: (Color online) Temperature range of the fluctuation regime  $|T_{JT} - T^*|$  (filled black spheres) and intra-dimer interaction  $J_0$  (open red squares, Ref. [17]) versus Sr content  $x$  in  $\text{Ba}_{3-x}\text{Sr}_x\text{Cr}_2\text{O}_8$ . Lines in the respective color indicate a linear dependence of these quantities on the Sr content  $x$  for comparison.

Lattice dynamics can be present in the hexagonal lattice in order to achieve a thermodynamically favoured orbitally non-degenerate ground state of a Jahn-Teller active ion in a distorted environment. Similar to  $\text{Ba}_{3-x}\text{Sr}_x\text{Cr}_2\text{O}_8$ , a dynamical transition has been observed in different materials, such as  $\text{BaNa}_2\text{Fe}[\text{VO}_4]_2$  where the transition is induced by the gradual evolution of the distortion around  $\text{FeO}_6$  [24]. Another example of dynamical orbital correlation is the spin state transition in  $\text{LaCoO}_3$  where the state changes gradually due to short-range orbital order [4]. A strong suppression of the Jahn-Teller-type crystal field with the lowering of structural symmetry was found in oxides such as  $\text{LaVO}_3$  upon cooling [26]. Moreover,  $\text{KCuF}_3$ , a material with Kugel-Khomskii-type orbital order and similar to high- $T_c$  superconducting cuprate perovskites, exhibits a large temperature range of structural fluctuations starting at the high-temperature structural transition, and extending down to the lower structural transition, which corresponds to a freezing of the octahedral rotations [6].

## CONCLUSIONS

Our heat capacity, Raman scattering, neutron and X-ray diffraction experiments reveal an extended orbit-lattice fluc-

tuation regime that depends on Sr/Ba concentration. Orbital ordering with suppressed orbital fluctuations is found to be reached far below the structural Jahn-Teller transition  $T_{JT}$  in  $x = 2.9$  and  $x = 2.8$ . Our investigations demonstrate the stabilization of the monoclinic  $C2/c$  space-group symmetry below a characteristic temperature  $T^*$  in  $\text{Ba}_{3-x}\text{Sr}_x\text{Cr}_2\text{O}_8$ . The Raman spectra change drastically with decreasing temperatures and the coherent part of lattice distortions develops only at lower temperatures.

The *dynamic* structural phase distortion discussed here is caused by strong orbital fluctuations. We have discussed different scenarios leading to a decrease in  $T_{JT}$  and the suppression of the fluctuation regime upon increasing Ba content. We conclude that a strong interdimer magnetic exchange interaction in the spin dimer network could support the fast stabilization of the orbit-lattice state, whereas large values of  $J_0$  lead to individual decoupled dimers, making the system more susceptible to fluctuations. Therefore, small modifications in the three dimensional magnetic exchange interactions could be of more crucial importance to stabilize different structural/orbital states in spin-charge-orbital couple systems, e.g. cuprates, manganites, ferrites, etc., than small changes in unit cell volumes or atomic positions.

We thank B. Lake for the access to the crystal growth laboratory, A. T. M. Nazmul Islam for the technical assistance, and the Helmholtz Zentrum Berlin for the access to neutron beam time at the research reactor BER II. We thank D. Chernyshov for the discussion and measurements at Swiss-Norwegian beamline BM01 at the ESRF in Grenoble. We thank G. Thorkildsen and O. Zavorotynska for useful discussion. A.G. is supported by the Swiss National Science Foundation Grant No. 21-153659. D.W. acknowledges financial support from the Quantum- and Nano-Metrology (QUANOMET) initiative within project NL-4.

---

\* alsu@physik.uzh.ch

- [1] J. Varignon, N. C. Bristowe, E. Bousquet and P. Ghosez, *Scientific Reports* **5**, 15364 (2015)
- [2] A. Stroppa, P. Barone, P. Jain, J. M. Perez-Mato, and S. Picozzi, *Adv. Materials* **25**, 2284 (2013)
- [3] A. Kyono, S. A. Gramsch, Y. Nakamoto, M. Sakata, M. Kato, T. Tamura and T. Yamanaka, *American Mineralogist* **100**, 1752 (2015)
- [4] Y. Tokura and N. Nagaosa, *Science* **288**, 5465 (2000)
- [5] H. Keller, A. Bussmann-Holder, and K. A. Miller, *Materials today* **11**, 9, 38-46 (2008)
- [6] J. C. T. Lee, Shi Yuan, et al., *Nature Physics* **8**, 63-66 (2012)
- [7] S. Pal and S. Lal, *Phys. Rev. B* **96**, 075139 (2017)
- [8] D. Wulferding, P. Lemmens, K.-Y. Choi, V. Gnezdilov, Y. G. Pashkevich, J. Deisenhofer, D. Quintero-Castro, A. T. M. Nazmul Islam, and B. Lake, *Phys. Rev. B* **84**, 064419 (2011)
- [9] L. C. Chapon, C. Stock, P. G. Radaelli, and C. Martin, arXiv:0807.0877v2.
- [10] Z. Wang, M. Schmidt, A. Günther, F. Mayr, Y. Wan, S.-H. Lee, H. Ueda, Y. Ueda, A. Loidl, and J. Deisenhofer, *Phys. Rev. B* **85**, 224304 (2012).
- [11] D. L. Quintero-Castro, B. Lake, E. M. Wheeler, A. T. M. N. Islam, T. Guidi, K. C. Rule, Z. Izaola, M. Russina, K. Kiefer, Y. Skourski, and T. Herrmannsdorfer, *Phys. Rev. B* **81**, 014415 (2010).
- [12] M. Kofu, H. Ueda, H. Nojiri, Y. Oshima, T. Zenmoto, K. C. Rule, S. Gerischer, B. Lake, C. D. Batista, Y. Ueda, and S.-H. Lee, *Phys. Rev. Lett.* **102**, 177204 (2009).
- [13] A. Zheludev, T. Roscilde, *Comptes Rendus Physique*, **14**, 740 (2013)
- [14] R. Maezono, S. Ishihara, and N. Nagaosa, *Phys. Rev. B* **58**, 11583 (1998).
- [15] J.-Q. Yan, J.-S. Zhou, and J. B. Goodenough, *Phys. Rev. Lett.* **93**, 235901 (2004)
- [16] Elbio Dagotto, *Science* **309**, 5732, 257-262 (2005).
- [17] A. Gazizulina, D. L. Quintero-Castro, and A. Schilling, *Phys. Rev. B* **96**, 184201 (2017)
- [18] H. Grundmann, A. Sabitova, A. Schilling, F. von Rohr, T. Forster, L. Peters, *New J. Phys.*, **18**, 033001 (2016)
- [19] H. Grundmann, A. Schilling, C.A. Marjerrison, H.A. Dabkowska, B.D. Gaulin, *Mat. Res. Bull.*, **48**, 3108 (2013)
- [20] Dyadkin, V., Pattison, Ph., Dmitriev, V., Chernyshov, L J. *Synchrotron Rad.*, **23**, 3 (2016)
- [21] J. Rodriguez-Carvajal, *Physica B.*, **192**, 55 (1993).
- [22] H. Grundmann, A. Schilling, M. Medarde, and D. Sheptyakov, *Phys. Rev. B* **90**, 075101 (2014)
- [23] G. Radtke, A. Saul, H. A. Dabkowska, G. M. Luke, and G. A. Botton, *Phys. Rev. Lett.* **105**, 036401 (2010)
- [24] Anna Reuss, Vadim Ksenofontov, Joshua Tapp et al., *Inorganic Chemistry*, **57**, 6300 (2018)
- [25] D. P. Landau, In *Theory of Magnetic Phase Transitions*; Kronmüller, H., Parkin, S., Eds.; *Handbook of Magnetism and Advanced Magnetic Materials. Fundamentals and Theory*; John Wiley and Sons, Ltd., 2007; Vol. 1
- [26] Minjae Kim and B. I. Min, *Phys. Rev. B* **89** 121106(R) (2014)